Barrier to Methyl Internal Rotation of 1-Methylvinoxy Radical in the $\tilde{X}(^2A'')$ and $\tilde{B}(^2A'')$ States: Experiment and Theory†

Sarah Williams,‡ Lawrence B. Harding,§ John F. Stanton,|| and James C. Weisshaar*,‡

Department of Chemistry, University of Wisconsin-Madison, Madison, Wisconsin 53706-1396, Chemistry Division, Argonne National Laboratory, Argonne, Illinois 60439, and Institute of Theoretical Chemistry, Department of Chemistry and Biochemistry, University of Texas at Austin, Austin, Texas 78712

Received: March 16, 2000; In Final Form: May 11, 2000

The jet-cooled laser induced fluorescence spectrum of the $\tilde{B} \leftarrow \tilde{X}$ electronic transition of the 1-methylvinoxy radical is assigned, including both hot and cold bands. The barrier to methyl internal rotation in both $\tilde{X}$ and $\tilde{B}$ states is determined by fitting pure torsional transitions to a one-dimensional hindered-rotor model. The resulting 3-fold torsional barrier parameters are $V_3' = -740 \pm 30$ cm^{-1} for the $\tilde{B}$ state (minimum-energy conformation with one methyl CH bond cis to the frame CO bond) and $V_3'' = +130 \pm 30$ cm^{-1} for the $\tilde{X}$ state (methyl CH bond trans to CO). The intensity pattern clearly indicates a change in the preferred methyl conformation upon excitation, while ab initio calculations provide the absolute conformations in each state. A variety of ab initio methods including CASSCF, multireference CI, and coupled-cluster techniques were applied to both the $\tilde{X}$ and the $\tilde{B}$ states of 1-methylvinoxy. Only the largest coupled-cluster calculations yield a $\tilde{B}$-state barrier in good quantitative agreement with experiment. In unsubstituted vinoxy, a $\tilde{B}$-state geometry adjusted earlier to fit experimental rotational constants (ref 10) is evidently in error.

I. Introduction

In combustion chemistry, substituted vinoxy radicals are primary products of reactions of O(^{3}P) atoms with alkenes.[1,2] Our recently reported jet-cooled laser induced fluorescence (LIF) spectra[3] of the $\tilde{B} \leftarrow \tilde{X}$ transition of 1-methylvinoxy (Figure 1) and of a mixture of *cis*- and *trans*-2-methylvinoxy have proven useful in identifying such primary reaction pathways. Similar spectra have been observed in flow-tube kinetics experiments and in a beam-plus-gas arrangement.[1,4]

The nature of the barrier to internal rotation of methyl groups and other alkyl groups adjacent to radical centers is an important topic in its own right. Such barriers influence the stereochemistry of radical reaction products. Methyl rotors attached to nonplanar radical-containing molecular frames have substantial barriers due to *hyperconjugation*, electron donation into the half-filled orbital vicinal to the methyl CH bonds.[5] In the series $CH_3CH_2^•$ to $CH_3CHF^•$ to $CH_3CF_2^•$, the calculated rotor barrier (UHF/aug-cc-pVDZ) increases from 53 to 720 cm^{-1} to 871 cm^{-1}, corresponding to increasing pucker about the central carbon atom. The planar ethyl radical has only a 17 cm^{-1} 6-fold barrier.[6] In contrast, the planar, symmetric frame of methylcyclopentadienyl radical induces only a small, 48 cm^{-1} barrier in the ground state.[7] The present example of 1-methylvinoxy in its $\tilde{X}$ and $\tilde{B}$ electronic states involves a planar frame lacking C_2 symmetry, as the methyl sits between one CC and one CO bond.

In this paper, we present a detailed assignment and analysis of the 1-methylvinoxy spectrum. Cold-band structure near the $\tilde{B}$-state origin yields the magnitude of the barrier to internal methyl rotation in the upper electronic state as well as frequency estimates for a number of active vibrational modes. Hot-band structure yields the same for the ground state. The remarkable complexity of the spectrum compared with that of unsubstituted vinoxy[8−10] is due primarily to a change in the preferred methyl rotor orientation on electronic excitation. With help from extensive electronic structure calculations, we conclude that the preferred conformation places one methyl CH bond cis to the CO bond in the $\tilde{X}$ state (130 ± 30 cm^{-1} barrier height) but trans to the CO bond in the $\tilde{B}$ state (740 ± 30 cm^{-1} barrier height).

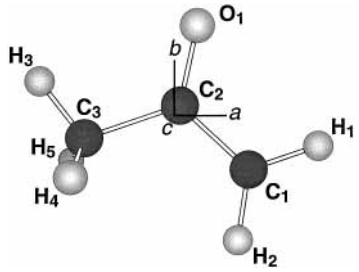

Figure 1. 1-Methylvinoxy geometry and atomic labeling scheme, with principal axes as shown.

In an attempt to interpret this dramatic shift in barrier with electronic excitation, we present a series of ab initio electronic structure calculations including complete-active-space self-consistent field methods (CASSCF), multireference configuration interaction methods (CAS+1+2), and coupled-cluster methods (CC) with a variety of basis sets. We find the $\tilde{B}$-state methyl rotor barrier to be remarkably difficult to compute accurately. Calculations that reproduce experimental $\tilde{B} \leftarrow \tilde{X}$ electronic transition energies and $\tilde{B}$-state vibrational frequencies quite well can still do poorly on the methyl rotor barrier. This is in sharp contrast with ab initio results for methyl rotor barriers in ground-state neutral and cationic substituted toluenes.[11] In 1-methylvinoxy, the changes in frame CC and CO bond orders on electronic excitation only partly explain the change in the methyl torsional potential.

† Part of the special issue "C. Bradley Moore Festschrift".

* Author to whom correspondence should be addressed. E-mail: weisshaar@chem.wisc.edu.

‡ University of Wisconsin-Madison.

§ Argonne National Laboratory.

|| University of Texas at Austin.

10.1021/jp001009q CCC: $19.00
Published on Web 06/21/2000

II. Experiment

The experimental apparatus has been described in detail elsewhere.[3] Briefly, the 1-methylvinoxy radicals are prepared by 193-nm photolysis of methyl isopropenyl ether, $CH_2{=}C(CH_3)OCH_3$, at the nozzle of a pulsed jet expansion of 2−3 atm Ar through a 1-mm-diameter nozzle. The radicals are probed 7 cm downstream with a frequency doubled Nd:YAG pumped dye laser near 357 nm (pulse width, 10 ns fwhm; bandwidth, 0.2 cm^{-1} fwhm; typical pulse energy, 2 mJ/pulse). A photomultiplier tube perpendicular to both the probe laser and the axis of the pulsed jet detects the resulting fluorescence. The resulting LIF spectra have not been normalized to laser power, which varies by roughly ±20% over the frequency range of interest, 27 200−29 600 cm^{-1}. Band positions are measured as the intensity maxima; reported absolute frequencies are accurate to ±2 cm^{-1}. The narrowest bands are 8 cm^{-1} fwhm, with differences in band frequencies accurate to ±0.6 cm^{-1}.

The degree of vibrational cooling of the radicals can be coarsely adjusted by changing the time interval between the firing of the photolysis and probe lasers, which varies the part of the photolyzed gas packet that is probed. Probing the radicals that were generated nearest the nozzle face produces the coldest spectra, whereas probing toward the leading edge of the packet gives vibrationally warmer spectra. Hot bands can thus be distinguished from cold bands. The coldest spectra are used to probe the methyl torsional potential of the $\tilde{B}$ state, whereas the hot bands from warmer spectra provide analogous information about the $\tilde{X}$ state.

III. Spectroscopic Background

A. Selection Rules. The well-studied $\tilde{B} \leftarrow \tilde{X}$ electronic spectrum of the vinoxy radical itself, as well as its fluoro- and methyl-substituted analogues, are examples of $\pi^* \leftarrow \pi$ transitions with both states of $^2A''$ symmetry.[3,4,8,12] In 1-methylvinoxy, the placement of a methyl CH bond in the plane of the molecule allows classification under the C_s point group. Because the methyl torsional motion is feasible on experimental time scales, the internal symmetry is higher than that of the point-group symmetry. The molecular Hamiltonian can thus be defined in a symmetry allowing for all energetically feasible permutations and permutation−inversions of equivalent nuclei.[13,14] For 1-methylvinoxy the molecular states are classified according to the irreducible representations of the molecular symmetry group G_6, which is isomorphic to the C_{3v} molecular point group.

Under G_6, the $\tilde{B} \leftarrow \tilde{X}$ electronic transition is $A_1 \leftarrow A_1$. Translations along the principal axes *a*, *b*, and *c* (Figure 1) transform as a_1, a_1, and a_2, respectively. The $\tilde{B} \leftarrow \tilde{X}$ electronic transition is, therefore, allowed and polarized in the plane of the vinoxy skeleton, resulting in AB-type hybrid bands. The appropriate symmetry labels for the pure torsional levels of 1-methylvinoxy are a_1, a_2, and *e*. As is customary, we label each stack of torsional states $0a_1$, $1e$, $2e$, $3a_2$, $3a_1$, $4e$, $5e$, $6a_2$, $6a_1$, and $7e$ in order of increasing torsional energy. The Franck−Condon allowed pure torsional transitions then follow the selection rules: $a_1 \leftrightarrow a_1$, $a_2 \leftrightarrow a_2$, and $e \leftrightarrow e$. These should be the strongest bands observed near the $\tilde{B}$-state origin. At higher energy in the $\tilde{B}$ state, we expect mixing of pure torsional states with low-frequency vibrational states and with torsion−vibration combination states, as well as the onset of new Franck−Condon-active vibrations and their associated torsional states. The spectral complexity can thus increase dramatically with $\tilde{B}$ state energy.

On the basis of experience with similar systems,[15−17] the conditions of the expansion in our experiment should effectively relax the 300 K torsional population distributions to the lowest spin-allowed level, i.e., $0a_1$ for all *a*-symmetry levels and $1e$ for all *e*-symmetry levels. By conservation of nuclear spin symmetry, the *a* and *e* levels do not interconvert. In this limit, the singly degenerate *a* torsional levels and the doubly degenerate *e* torsional levels of the methyl group have equal nuclear spin statistical weight factors.

B. Torsional States and Spectral Fitting. To solve the hindered internal rotation problem, we treat the methyl group and molecular frame as rigid rotors. Neglecting overall rotation and torsion−rotation coupling, the torsional Hamiltonian can be written in its simplest form[18]

$$H(\alpha) = -Fp^2 + V(\alpha) \tag{1}$$

where F is the reduced rotational constant for the methyl group relative to the H_2CCO molecular frame, α is the torsional angle as referenced to the frame, and p is the torsional angular momentum conjugate to α. We define $\alpha = 0$ as the conformation with one methyl CH bond in the plane of the molecular frame cis to the CO bond, as in Figure 1. Because the methyl rotor top axis does not coincide with any of the principal axes of the molecule, F is given by $^1/_2 r I_\alpha$. Here, I_α is the moment of inertia of the $-CH_3$ top about its symmetry axis and $r = 1 - I_\alpha(\lambda_a^2/I_a + \lambda_b^2/I_b + \lambda_c^2/I_c)$, where I_a , I_b, and I_c are the principal moments of inertia for the entire molecule including the methyl group; and λ_a, λ_b, and λ_c are the direction cosines between the inertial axes and the methyl top axis of rotation. $V(\alpha)$ is the one-dimensional torsional potential modeled by using the conventional symmetry-adapted Fourier expansion.

$$V(\alpha) = \sum_n \frac{V_{3n}}{2}(1 - \cos 3n\alpha) \qquad n = 0, 1, 2, ... \tag{2}$$

Because this expansion converges rapidly, it is generally appropriate to neglect terms higher than $n = 2$.

For the $\tilde{B}$ state of 1-methylvinoxy, the data will allow us to determine a 3-fold term V_3' and a small 6-fold term V_6'. For the $\tilde{X}$ state, we will determine only V_3''. In each case, $|V_3|$ gives the magnitude of the barrier to internal rotation. For $V_6 \ll V_3$, the small 6-fold term controls the width of the barrier. The sign of V_3 fixes the lowest-energy conformation. With our choice of $\alpha = 0$ (Figure 1), for $V_3 > 0$, the potential minima lie at $\alpha = 0°$, 120°, and 240° in what we call the cis conformation. For $V_3 < 0$, the potential minima occur at $\alpha = 60°$, 180°, and 300° in the trans conformation. Unlike pure 6-fold cases in which the torsional barriers are very small, the 3-fold barriers typically encountered localize probability density for the lowest levels in the potential wells. In the limit of a large barrier, pairs of *a* and *e* levels converge in energy to become 3-fold degenerate vibrational levels as follows: $0a_1$ and $1e \rightarrow \upsilon = 0$; $2e$ and $3a_2 \rightarrow \upsilon = 1$; and $3a_1$ and $4e \rightarrow \upsilon = 2$; etc.

To model the spectra, we diagonalize the Hamiltonian in a basis set of 80 free rotor eigenfunctions ($e^{im\phi}$, $m = 0, \pm1, \pm2, ...$), as before.[19] The matrix elements are

$$H_{m,m'} = Fm^2\delta_{m,m'}$$

$$H_{m,m'\pm3} = -\frac{V_3}{4}\delta_{m,m'\pm3}$$

$$H_{m,m'\pm6} = -\frac{V_6}{4}\delta_{m,m'\pm6} \tag{3}$$

We first determine the best $\tilde{B}$-state parameters from the

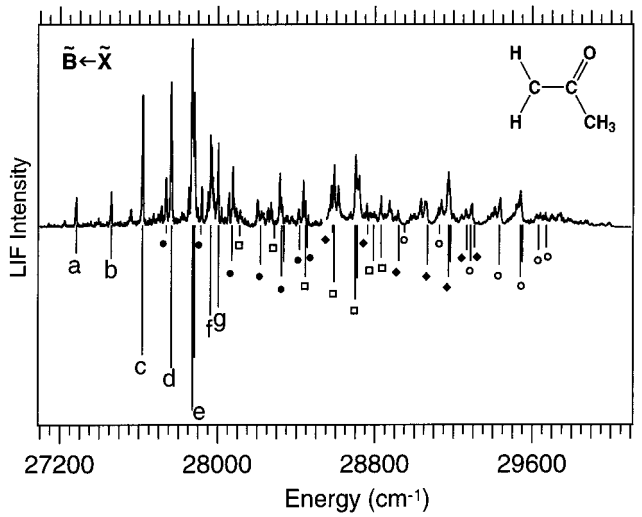

Figure 2. Top: $\tilde{B} \leftarrow \tilde{X}$ LIF spectrum of 1-methylvinoxy. Bottom: repetitions of $a-b-c-d-e-f-g$ torsional envelope to match spectrum. Each symbol denotes a torsional progression atop a different excited-state vibration (Table 2). Filled circles, OC_2C_1 bend (454 cm^{-1}); open squares, $OC_2C_1C_3$ breathing (829 cm^{-1}); diamonds, C_1C_2 stretch (1303 cm^{-1}); and open circles, C_1O stretch (1668 cm^{-1}).

vibrationally cold spectrum with V_3'' fixed at 130 cm^{-1}, as described below. This fitting procedure is not very sensitive to the choice of $\tilde{X}$-state parameters as long as V_3'' is larger than about 100 cm^{-1} and the proper change in the potential minimum from $\tilde{X}$ to $\tilde{B}$ is included. With V_3' and V_6' frozen at the best values, we then determine V_3'' from the hot bands measured in the vibrationally hot spectrum.

Judging from earlier work, we expect the simple one-dimensional model of internal rotation to work best at low excitation energies in each electronic state. It has been especially effective below the energy of the first molecular vibration, which occurs at about 400 cm^{-1} in 1-methylvinoxy. At higher energy, the onset of a variety of torsional−vibrational coupling mechanisms typically produces extra bands and/or perturbs the positions of nominally pure torsional bands. We will find that 1-methylvinoxy follows this pattern.

IV. Experimental Results

A. Cold Bands. The $\tilde{B} \leftarrow \tilde{X}$ LIF spectrum of 1-methylvinoxy spans the range 27 282−30 000 cm^{-1} and consists of over 50 vibronic bands (Figure 2). A detailed list of frequencies of all of the stronger bands is included in ref 3. In comparison, the $\tilde{B} \leftarrow \tilde{X}$ LIF spectrum of plain vinoxy consists of about seven strong bands spanning the range 28 785−30 200 cm^{-1} before the intensity drops significantly. We will argue convincingly that the $\tilde{B} \leftarrow \tilde{X}$ origin is band *a* at 27 282.5 cm^{-1} for 1-methylvinoxy, a 1502 cm^{-1} shift from the value of 28 784.1 cm^{-1} for plain vinoxy. In both cases the LIF spectra die off at higher energy because of rapidly decreasing lifetimes, as described earlier.[3,8,20] In plain vinoxy, the most significant geometry change in the $\tilde{B} \leftarrow \tilde{X}$ electronic transition is the lengthening of the CO bond,[8,10,21] and we expect a similar change in geometry in 1-methylvinoxy. However, the sheer number of bands in the 1-methylvinoxy spectrum then strongly suggests an additional change in the preferred methyl rotor conformation upon excitation.

The intensity envelope of the lowest-energy bands also suggests a conformational change in the methyl group. Figure 3 shows an expanded view of what we assign as the first torsional envelope of the 1-methylvinoxy spectrum. We fit both

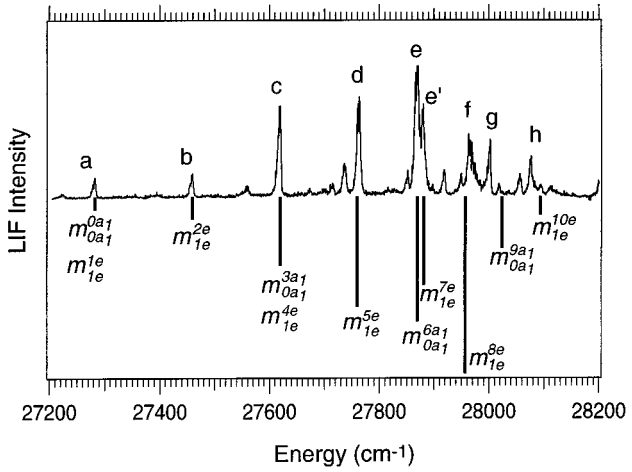

Figure 3. Expanded view of first torsional envelope of $\tilde{B} \leftarrow \tilde{X}$ LIF spectrum juxtaposed with a stick representation of the fit to the one-dimensional torsional model for the $\tilde{B}$ state. Parameters of this fit in Table 1. See text for details.

TABLE 1: 1-Methylvinoxy $\tilde{B}$-State Assignments

		energy[a]	$\tilde{B}$-state		intensity	
band	assign.	(cm^{-1})	expt.[b]	calc.[c]	expt.[b]	calc.[c]
a	$m_{0a_1}^{0a_1}$, m_{1e}^{1e}	27282.5	0	0	1	1
b	m_{1e}^{2e}	27459.4	176.9	176.8	1	1
c	$m_{0a_1}^{3a_1}$, m_{1e}^{4e}	27617.5	335	336.8, 336.9	5	4
d	m_{1e}^{5e}	27763.2	480.7	477.2	6	9
e	$m_{0a_1}^{6a_1}$	27868.8	586.3	586.0	9	9
e′	m_{1e}^{7e}	27880.7	598.2	599.3	6	6
f	m_{1e}^{8e}	27962.9	680.4	674.2	7	12
g	$m_{0a_1}^{9a_1}$	28002.1	719.6	743.0	3	3
h	m_{1e}^{10e}	28076.4	793.9	815.4	2	1

[a] See ref 3 for frequencies of all additional strong bands. Accuracy ±2 cm^{-1}. [b] Accuracy ±0.6 cm^{-1} for frequencies, ±30% for relative intensities. [c] Model parameters: $V_3' = -751$ cm^{-1}, $V_6' = 26$ cm^{-1}, and $F' = 4.8$ cm^{-1}; and $V_3'' = 130$ cm^{-1}, $V_6'' = 0$ cm^{-1}, and $F'' = 5.2$ cm^{-1}. Intensities are scaled Franck−Condon factors.

the frequencies and intensities of the $a-b-c-d-e-f$ pattern of bands to the one-dimensional torsional Hamiltonian of eqs 2 and 3. Our fitting procedure includes three adjustable parameters for the $\tilde{B}$ state: F', V_3', and V_6'. The $\tilde{X}$-state barrier is frozen at 130 cm^{-1} with the sign of V_3'' opposite to that of V_3' to produce the broad envelope of strong torsional transitions. The frequencies of the $a-b-c-d-e-f$ bands of Figure 3 (including the splitting in the *e* band assigned to the $6a_1$ and $7e$ transitions) were optimized by searching a three-dimensional grid of values for the best F', V_3', and V_6' combination, as determined by the χ^2 parameter. The values of F' were constrained to the physically realistic range 4.5−6.0 cm^{-1}.[22,23] Two regions of parameter space give comparably good fits to the frequencies and intensities. The two regions are centered around the values $F' = 4.8$ cm^{-1}, $V_3' = -751$ cm^{-1}, and $V_6' = 26$ cm^{-1} and $F' = 5.2$ cm^{-1}, $V_3' = -735$ cm^{-1}, and $V_6' = 10$ cm^{-1}. The first set of parameters is somewhat preferred, as it predicts the torsional frequencies slightly better. These are the values used in the fits presented in the tables and the figures. Our conservative best estimates of the fitted potential parameters span both regions: $V_3' = -740 \pm 30$ cm^{-1} and $V_6' = 20 \pm 15$ cm^{-1}. The fit frequencies and intensities are compared with those from experiment in Table 1.

As shown in Figure 3, the fit to both intensities and frequencies is excellent up to bands *e* and *e*′, but degrades for

TABLE 2: $\tilde{B}$-state Vibrational Energies for 1-Methylvinoxy and Unsubstituted Vinoxy[a]

	1-methylvinoxy				vinoxy	
description	expt.[b]	calc.[c]	calc.[d]	calc.[e]	expt.[f]	calc.[g]
OC_2C1 bend	454	474	450	439	449	480
$OC_2C_1C_3$ breathing	829	856	850	845	–	–
C_1C_2 stretch	1303	1409	1370	1394	917	998
C_1O stretch	1668	1894	1830	1830	1621	1881

[a] See Figure 1 for atom numbering. All energies in cm^{-1}. Calculated frequencies are unscaled. [b] Estimated accuracy ± 25 cm^{-1}. [c] CASSCF(5,4)/6-31G**. [d] (3,3)-CAS+1+2/cc-pVDZ (rounded to nearest 10 cm^{-1}). [e] QRHF-EOMEE-CCSD/cc-pVDZ. [f] Ref 8. [g] Ref 25.

f−*h*. Most of the smaller unassigned bands in the range *a*−*e*′ will be explained as hot bands below. Calculated bands in the vicinity of experimental bands *f*−*h* reach to 600 cm^{-1} and beyond in the $\tilde{B}$ state (near the top of the barrier) and span a clump of experimental bands of roughly the right overall intensity. We suspect that coupling of pure torsional states to torsion−vibration states of the same overall tv symmetry has begun, much as is observed in other molecules.[19,24]

The intensities easily allow us to determine that a change in preferred conformation has occurred upon excitation, but we cannot determine the absolute methyl conformation experimentally. That is determined by theory in section V below. All of the computational work corroborates the change in preferred conformation and consistently finds that the $\tilde{X}$-state minimum places one methyl rotor CH bond cis to the CO bond ($\alpha = 0°$, positive V_3''). In the $\tilde{B}$ state, the minimum places one methyl CH bond trans to the CO bond ($\alpha = 180°$, negative V_3').

The fit of the first torsional envelope then permits a semiquantitative understanding of the complete spectrum and extraction of *approximate* $\tilde{B}$-state vibrational frequencies. Assuming that the methyl rotor potential is essentially independent of vibrational state, every vibrational transition should repeat this torsional envelope as a series of combination bands of vibrational and torsional mode quanta. In Figure 2, we juxtapose the entire 1-methylvinoxy $\tilde{B}$-state LIF spectrum with a series of torsional envelopes repeated to fit what we believe to be the strongest vibrational transitions of the radical. This fit was performed by eye, using a stick representation of the first torsional envelope *a*−*b*−*c*−*d*−*e*−*f* based on the actual torsional frequencies and intensities in the spectrum and seeking series of bands throughout the spectrum that repeat the entire pattern. The intensity of the *e* band of each envelope was normalized to the band in the spectrum to which it was assigned. The $\tilde{B}$-state vibrational levels estimated from this procedure are collected in Table 2. They, in fact, agree reasonably well with those determined from ab initio work on 1-methylvinoxy (section V) and are also quite reminiscent of the most active modes in the $\tilde{B} \leftarrow \tilde{X}$ LIF spectrum of plain vinoxy (also in Table 2). Although the fit reproduces the overall shape of the entire spectrum and accounts for the majority of the bands, it does not account for every band and small discrepancies in frequency and intensity do exist. As vibrational energy increases, perturbations surely arise because of the increasing density of torsional-vibrational states, leading to modest discrepancies. The effective V_3' and F' values may vary slightly with vibrational state as well. The accuracy of vibrational frequencies estimated in this way is about $\pm$ 25 cm^{-1}.

B. Hot Bands. In efficiently cooled spectra (Figures 2 and 3), the transitions arise predominantly from the $0a_1$ and $1e$ torsional levels in the ground state. These cold spectra exhibit several additional weak bands at low energy not accounted for by our *a*−*b*−*c*−*d*−*e*−*f* torsional model. In vibrationally warmer spectra, these unassigned weak bands broaden toward lower frequency and increase in intensity (Figure 4). No additional bands were observed below 27 180 cm^{-1}. We measure the frequencies of the broad bands at the intensity maxima. They can be readily assigned as torsional hot bands arising from the $2e$, $3a_2$, and $3a_1$ levels of the $\tilde{X}$ state. These transitions were fit to the one-dimensional rigid rotor Hamiltonian by the same procedure as described previously, with the $\tilde{B}$-state parameters $F' = 4.8$ cm^{-1}, $V_3' = -751$ cm^{-1}, and $V_6' = 26$ cm^{-1} frozen at the values determined from the cold spectrum. The best fit parameters are $F'' = 5.2 \pm 0.4$ cm^{-1} and $V_3'' = 130 \pm 20$ cm^{-1}. The V_6'' term was not included as it cannot be well determined. Figure 4 shows the fit of the hot bands for $F'' = 5.2$ cm^{-1} and $V_3'' = 130$ cm^{-1}. Relative intensities of transitions arising from the same torsional state in the ground state are taken to be proportional to the model Franck−Condon factors. The initial transition of each series is adjusted to match the experimental intensity to which it is being fit. The hot band spectrum not only provides information about the $\tilde{B}$ state, but also corroborates the $\tilde{B}$-state assignments, as the hot bands observed are consistent with the selection rules governing the $\tilde{B} \leftarrow \tilde{X}$ transitions between torsional states ($a_1 \leftarrow a_1$, $a_2 \leftarrow a_2$, $e \leftarrow e$). Table 3 shows the comparison between experimental $\tilde{X}$-state torsional frequencies and intensities and those from the fit.

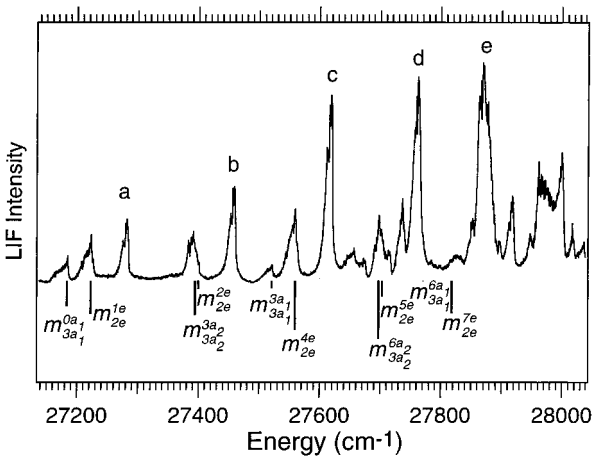

Figure 4. Expanded view of the first torsional envelope of a warmer $\tilde{B} \leftarrow \tilde{X}$ LIF spectrum than in Figure 3. Stick spectrum and assignments below are based on a one-dimensional torsional fit to the $\tilde{X}$ state. Parameters of this fit in Table 3.

TABLE 3: 1-Methylvinoxy Hot Bands and Assignments

	energy (cm^{-1})		intensity	
assign.	expt.[a]	calc.[b]	expt.[a]	calc.[b]
m^{1e}_{2e}	27223	27222	1	1
m^{2e}_{2e}		27398		0.2
m^{4e}_{2e}	27560	27557	2.3	1.1
m^{5e}_{2e}		27702		0.3
$m^{3a_2}_{3a_2}$	27391	27390	1	1
$m^{6a_2}_{3a_2}$	27698	27693	1.5	1.5
$m^{0a_1}_{3a_1}$	27184	27184	1	1
$m^{3a_1}_{3a_1}$	27520	27519	0.5	0.2
$m^{6a_1}_{3a_1}$		27771		~0.04

[a] Energies measured at peak intensities accurate to ± 5 cm^{-1}. Intensities accurate to $\pm$30%. [b] Model parameters: $V_3' = -751$ cm^{-1}, $V_6' = 26$ cm^{-1}, and $F' = 4.8$ cm^{-1}; and $V_3'' = 130$ cm^{-1}, $V_6'' = 0$ cm^{-1}, $F'' = 5.2$ cm^{-1}. Intensities are scaled Franck−Condon factors.

TABLE 4: Threefold Ab Initio Barriers V_3 (cm^{-1})[a] for $\tilde{B}$- and $\tilde{X}$-State 1-Methylvinoxy Radical at Different Levels of Theory

method[b]	$\tilde{B}$-state	$\tilde{X}$-state
experiment	-740 ± 30	$+130 \pm 20$
1 (3,3)-CASSCF/cc-pVDZ[d]//**1**[d]	−196	230
2 (3,3)-CASSCF/aug-cc-pVDZ[d]//**1**[d]	−237	225
3 (3,3)-CASSCF/cc-pVTZ[d]//**1**[d]	−235	207
4 (5,4)-CASSCF/6-31G(d,p)e //**4**[e]	−193	195
5 (5,4)-CASSCF/6-31++G**[e]//**5**[e]	−239	
6 (3,3)-CAS+1+2/cc-pVDZ[d]//**1**[d]	−304 (−336)[c]	188 (175)[c]
7 (3,3)-CAS+1+2/aug-cc-pVDZ[d]//**1**[d]	−371 (−415)[c]	157 (131)[c]
8 (3,3)-CAS+1+2/cc-pVTZ[d]//**1**[d]	−371 (−415)[c]	142 (117)[c]
6[f]//**6**[f]	−350 (−413)[c]	180 (152)[c]
6[d]//**6**[d]	−322 (−365)[c]	187 (171)[c]
7[d]//**6**[d]	−388 (−445)[c]	158 (130)[c]
8[d]//**6**[d]	−392 (−453)[c]	
9 B-CCD/cc-pVDZ//**6**[f]	−686	
10 B-CCD(T)/cc-pVDZ//**6**[f]	−552	
11 QRHF-CCSD/cc-pVDZ//**6**[f]	−670	
12 QRHF-CCSD(T)/cc-pVDZ//**6**[f]	−606	
13 QRHF-CCSDT/cc-pVDZ//**6**[f]	−482	
14 QRHF-EOMEE-CCSD/cc-pVDZ//**6**[f]	−550	
14//**14**	−566	
15 QRHF-EOMEE-CCSD/cc-pVTZ//**6**[f]	−690	

[a] *Positive* V_3 places the potential minimum with a methyl CH bond cis to the OC bond ($\alpha = 0$), and *negative* V_3 places the minimum with the CH bond trans to the OC bond. [b] The notation **X**//**Y** means geometry optimization was carried out using the level of theory **Y** and the energy at that geometry was evaluated using level of theory **X**. [c] Includes Davidson correction (refs 38 and 39). [d] Calculations performed using Molpro (refs 32−34). [e] Calculations performed using Gaussian (ref 30). [f] Calculations performed using Columbus (ref 31).

V. Ab Initio Calculations

A. Overview of Methods. The unsubstituted vinoxy radical has been the subject of extensive theoretical work including complete-active-space self-consistent-field (CASSCF) excited-state calculations of the $\tilde{B}$ state.[21,25,26] Our first ab initio calculations on 1-methylvinoxy used the CASSCF method based on similar calculations on vinoxy by Rohlfing.[25] As with vinoxy, this method provided reasonable agreement with experiment for excitation energies and vibrational frequencies. However, CASSCF resulted in a large discrepancy between calculated and experimentally determined methyl rotor barriers. Therefore we explored multireference CI calculations based on the CAS wave function and also a variety of coupled-cluster calculations. As detailed in Table 4, the bulk of the electronic structure calculations used three of the Dunning correlation-consistent basis sets: the double-ζ (cc-pVDZ), the augmented double-ζ (aug-cc-pVDZ) and the triple-ζ (cc-pVTZ) basis sets.[27−29] The exceptions are the GAUSSIAN 98[30] CASSCF calculations, which used the 6-31G** and the 6-31++G** basis sets. The CAS calculations used the program packages Columbus,[31] Molpro,[32−34] and Gaussian.[30] The coupled-cluster calculations used the version of the ACES II program system resident at the University of Texas-Austin.[35]

Three different reference wave functions were considered in the multireference calculations. The majority of the calculations employ a three-electron, three-orbital CAS reference wave function. The three active orbitals are the singly occupied radical orbital ($3a''$) and the CO π and π^* orbitals ($2a''$ and $4a''$). For the $\tilde{B}$ state, this reference wave function is workable only for geometries of C_s symmetry. For geometries of C_1 symmetry one needs to enlarge the reference space to include the oxygen lone-pair a' orbital. The (5,4) calculations listed in Table 4 and described later in this section use this active space including the oxygen lone-pair a' orbital and its two electrons. Using these reference configurations, two kinds of multireference, singles and doubles configuration interaction calculations were performed. Uncontracted CAS+1+2 calculations used the Columbus program,[31] and internally contracted, CAS+1+2 calculations used the Molpro program.[32,36,37] The effects of higher-order excitations (beyond singles and doubles) were examined using multireference Davidson corrections.[38,39]

We explored several different approaches based on the coupled-cluster (CC) approximation.[40−43] To avoid problems associated with variational collapse of the $\tilde{B}$ state in determination of the reference determinant, both Brueckner orbitals[44] and the quasi-restricted Hartree−Fock (QRHF) method of Rittby and Bartlett[45] were used. In the latter approach, orbitals were obtained in a Hartree−Fock calculation for the 1-methylvinoxy anion; one electron was then removed from the penultimate occupied a'' orbital and the resulting determinant was used in the CC calculations. Brueckner orbitals were easily obtained by using the QRHF orbitals as a starting approximation.

Both the Brueckner (B-CC) and QRHF-CC approaches are based on single determinant reference functions. Inspection of the resulting correlated wave functions obtained at the coupled-cluster doubles (B-CCD) and coupled-cluster singles and doubles (QRHF-CCSD) levels reveals that the most important configurations are those with the a'' orbital occupations $1a''^2 2a''^1 3a''^2 4a''^0$ (the reference determinant) and $1a''^2 2a''^2 3a''^0 4a''^1$. The extent of mixing between these two configurations is substantial. The corresponding double excitation amplitude is between 0.3 and 0.4, calling into question the propriety of using these usually quite reliable single-reference approaches.

As an alternative, the equation-of-motion coupled-cluster method for excited states (EOMEE-CC)[46] was used. In this approach, a calculation is performed for the ground electronic state, and excited states are obtained by diagonalization of a similarity-transformed Hamiltonian in a basis that consists of all single and double excitations relative to the single-determinant description for the *ground* electronic state. For 1-methylvinoxy, the ground-state determinant is that with the $1a''^2 2a''^2 3a''^1 4a''^0$ occupation of a'' orbitals; both of the important configurations for the $\tilde{B}$ state are related to this determinant by a single excitation. Hence, EOMEE-CC offers a balanced treatment of the important configurations that describe the $\tilde{B}$ state that is impossible to achieve with the usual single-reference CC methods using any choice of orbitals. Because problems were encountered in obtaining satisfactory Hartree−Fock solutions for the ground state of 1-methylvinoxy, QRHF orbitals were used.[47] The resulting calculations, which used the EOMEE-CC method in the singles and doubles approximation using a ground-state description based on QRHF orbitals, are called QRHF/EOMEE-CCSD in the following. Apart from the QRHF-CCSDT energies obtained for the $\tilde{B}$-state rotamers, for which the four lowest-lying (nominal carbon and oxygen 1s) orbitals were excluded in the treatment of electron correlation, no orbitals were frozen in any of the other CC calculations.

In all cases, the 3-fold potential parameter V_3 is estimated as the difference in energy between the conformation with $\alpha = 0°$ and the conformation with $\alpha = 180°$. Because geometry optimizations relaxed all other geometric parameters at $\alpha = 0°$ and 180°, we call these estimates the vibrationally adiabatic torsional barrier. Zero-point corrections to the vibrationally adiabatic barrier were applied at those levels of theory for which the geometry was optimized at both $\alpha = 0°$ and 180°. They were always small, 10−20 cm^{-1}, in both the $\tilde{X}$ and $\tilde{B}$ states.

B. Computational Results. The 3-fold rotational barriers V_3 determined by these methods are compiled in Table 4 for both the $\tilde{X}$ and the $\tilde{B}$ states. The notation of Table 4 follows the usual convention of listing the method of calculation to the left of the double slash and the method with which the geometry was optimized to the right. Although not the focus of our study, the adiabatic electronic excitation energy is 28 600 cm^{-1} at the uncontracted (3,3)-CAS+1+2 level. Using QRHF-CCSD for the ground state and QRHF/EOMEE-CCSD for the excited state with the cc-pVDZ basis set and CAS+1+2 geometries gives 29 400 cm^{-1}. Both values are in reasonable agreement with the experimental value of 27 282 cm^{-1}.

The majority of the theoretical models were used to determine the torsional barrier for the ground state of 1-methylvinoxy. The calculations on the ground state give V_3'' values that range from 230 to 117 cm^{-1}, compared with the experimental barrier of 130 ± 20 cm^{-1}. The more extensive basis sets and more complete methods are able to predict this barrier to within about 30 cm^{-1} when the Davidson correction is included.

A few ground-state calculations used coupled-cluster methods at the CAS+1+2 geometries; these results are not included in Table 4. Using unrestricted Hartree−Fock orbitals, V_3'' values of +172 and +115 cm^{-1} are obtained at the CCSD level using the cc-pVDZ and cc-pVTZ basis sets, respectively. Triple excitations have only a small effect; the corresponding CCSD-(T) barrier heights are +170 and +108 cm^{-1}. Although the unrestricted Hartree−Fock reference suffers from fairly severe spin contamination ($\langle S^2 \rangle = 0.95$ at the $\tilde{X}$-state geometries), it is widely appreciated that standard CC methods that include a full treatment of single excitations [such as CCSD and CCSD-(T)] are fairly insensitive to reference state spin contamination[47,48] when applied to the ground electronic state. In addition, CCSD and CCSD(T) calculations were performed with QRHF orbitals, which are not spin-contaminated. With the cc-pVDZ basis set, the QRHF-CCSD and QRHF-CCSD(T) results for V_3'' are +191 and +156 cm^{-1}, respectively. Taken as a whole, the CC results suggest a barrier height in the range 100−200 cm^{-1}, consistent with the experimental result.

For the $\tilde{B}$ state, regardless of basis set, the (3,3)-CASSCF and the (5,4)-CASSCF calculations give values for V_3' of roughly −200 cm^{-1}, some 500 cm^{-1} too small in magnitude compared with the experimental result of −751 cm^{-1}. The (3,3)-CAS+1+2 methods yield V_3 in the range −300 to −400 cm^{-1}, increasing to −400 to −450 cm^{-1} when the Davidson correction is included. The multireference CI methods at best reach only 60% of the experimental barrier in the excited state.

$\tilde{B}$-state rotational barriers obtained from single-point calculations with various CC methods at the optimized CAS+1+2 geometries more closely match experiment. Using the cc-pVDZ basis set, the Brueckner-based CCD and CCD(T) methods give V_3' parameters of −690 and −550 cm^{-1}, respectively. The corresponding QRHF-CCSD and QRHF-CCSD(T) results are −670 and −610 cm^{-1}. However, a *full* CCSDT calculation carried out with QRHF orbitals gives a substantially lower V_3' of −480 cm^{-1}. This effect is *not* due to the fact that the core orbitals were dropped in the CCSDT calculation, so it would appear that the perturbative treatment of triple excitations included in B-CCD(T) and QRHF-CCSD(T) is not very accurate in the present case.[49] However, when the more balanced QRHF/EOMEE-CCSD method is used, the barrier height of 550 cm^{-1} is intermediate between those obtained using QRHF-CCSD(T) and QRHF-CCSDT. Expansion of the basis to cc-pVTZ improves the calculated value to −690 cm^{-1}, which is in quite good agreement with the experimental determination.

TABLE 5: $\tilde{B}$-State Vinoxy Geometries[a]

				adjusted	
	calc. X[b]	calc. Y[c]	calc. Z[d]	ref 10[e]	this work[f]
$r(C_2O)$	1.360	1.375	1.378	1.337	1.38
$r(C_1C_2)$	1.450	1.446	1.434	1.466	1.43
$r(H_3C_2)$	1.075	1.094	1.100	1.069	1.09
$r(H_1C_1)$	1.072	1.088	1.094	1.069	1.09
$r(H_2C_1)$	1.071	1.087	1.093	1.069	1.09
$\angle OC_2C_1$	121.5	122.7	123.1	129.5	123.1
$\angle H_1C_1C_2$	120.1	120.0	120.1	120.0	120.0
$\angle H_2C_1C_2$	119.9	119.8	119.8	119.5	120.0
$\angle H_3C_2C_1$	116.8	120.4	120.1	120.9	120.0

[a] Atom labels based in Figure 1. Bond lengths in angstroms, angles in degrees. [b] CASSCF(3,3)/6-31G**, ref 25. [c] (3,3)-CAS+1+2/cc-pVDZ. [d] EOMEE-QRHF/cc-pVDZ. [e] From ref 10. [f] Values based on (3,3)-CAS+1+2/cc-pVDZ geometries, adjusted to fit experimental rotational constants from ref 10.

TABLE 6: $\tilde{B}$-State Rotational Constants (cm^{-1}) for Vinoxy Radical

					adjusted	
	expt.[a]	calc. X[b]	calc. Y[c]	calc. Z[d]	ref 10[a]	this work[e]
A (cm^{-1})	2.103 ± 0.004	2.069	2.0765	2.090	2.4287	2.1028
B (cm^{-1})	0.3442 ± 0.0012	0.3496	0.3429	0.343	0.3278	0.3441
C (cm^{-1})	0.2958 ± 0.0012	0.2991	0.2943	0.295	0.2888	0.2957

[a] From ref 10. [b] CASSCF(3,3)/6-31G**, ref 25. [c] (3,3)-CAS+1+2/cc-pVDZ, this work. [d] EOMEE-QRHF−CCSD/cc-pVDZ, this work. [e] Values from fit based on the (3,3)-CAS+1+2/cc-pVDZ calculation.

To estimate the vibrational contribution to V_3', both of the $\tilde{B}$-state rotamers were optimized at the QRHF/EOMEE-CCSD level[50] with the cc-pVDZ basis set; these structures were then used in a harmonic vibrational frequency calculations. The zero-point vibrational contribution to V_3' is about +20 cm^{-1}. Hence, the best coupled-cluster estimate of the vibrationally adiabatic V_3' parameter for the $\tilde{B}$ state is obtained from the QRHF/EOMEE-CCSD value with the cc-pVTZ basis set augmented by this small correction, i.e., $V_3' = -710$ cm^{-1}. This compares quite favorably with the experimental result of −740 ± 30 cm^{-1}.

VI. Discussion

A. $\tilde{B}$-State Geometry. For unsubstituted vinoxy radical, DiMauro et al.[10] obtained a high-resolution $\tilde{B} \leftarrow \tilde{X}$ LIF spectrum and accurate $\tilde{X}$- and $\tilde{B}$-state rotational constants. They subsequently adjusted two geometric parameters, the C_2O bond lengths and the angle C_1C_2O, in an effort to fit the $\tilde{B}$-state rotational constants. The rest of the geometric parameters used in the fitting procedure were taken from the calculations of Dupuis et al.[26] It appears that DiMauro's calculations were in error. Table 5 compares calculated $\tilde{B}$-state geometric parameters obtained by optimization at three levels of theory labeled X, Y, and Z (CASSCF, CAS+1+2, and QRHF/EOMEE-CCSD, respectively) with the adjusted $\tilde{B}$-state geometry from DiMauro et al. Table 6 shows the corresponding $\tilde{B}$-state rotational constants A, B, and C about the three principal inertial axes. The ab initio rotational constants agree with experiment increasingly well as more electron correlation is included. The CAS+1+2 and the QRHF/EOMEE-CCSD geometries are quite similar. The rotational constants from the QRHF/EOMEE-CCSD agree with all three experimental rotational constants to within 1%.

However, the adjusted geometry of DiMauro et al. gives rotational constants that disagree with experiment by 13% for A, 5% for B, and 2% for C. This suggests a problem with the

TABLE 7: Calculated 1-Methylvinoxy Geometries[a]

	$\tilde{X}$		$\tilde{B}$		
	calc. X[b]	calc. Y[c]	calc. X[b]	calc. Y[c]	calc. Z[d]
$r(C_1O)$	1.221	1.231	1.362	1.375	1.380
$r(C_1C_2)$	1.451	1.454	1.451	1.442	1.427
$r(C_3C_2)$	1.514	1.517	1.493	1.490	1.488
$\angle OC_2C_1$	120.2	120.5	120.1	121.7	122.7
$\angle C_1C_2C_3$	118.7	118.0	123.8	122.8	122.6

[a] All distances in angstroms and angles in degrees. [b] (5,4)-CASSCF/6-31G(d,p), this work. [c] (3,3)-CAS+1+2/cc-pVDZ, this work. [d] QRHF-EOMEE-CCSD/cc-pVDZ, this work.

calculations of ref 10; the rotational constants we compute from the geometry of DiMauro et al. (Table 6) do not agree with those in Table 2 of ref 10. The substantial problem about the *A* axis is closely related to the values of $r(C_2O)$ and $r(C_1C_2)$. The last columns of Tables 5 and 6 show a set of geometric variables slightly adjusted from the ab initio values and the corresponding rotational constants. The agreement with experiment falls within its uncertainty, lending credibility to the ab initio geometry. Such an adjustment is, of course, not unique.

For 1-methylvinoxy, the ab initio geometry of the frame is given in Table 7 for two levels of theory in the $\tilde{X}$ state and for three levels of theory in the $\tilde{B}$ state. For the ground state, the CASSCF and CAS+1+2 geometries are quite similar. For the $\tilde{B}$ state, the frame geometry changes significantly as correlation effects are added. The C_2O bond length increases, and the frame C_1C_2 bond length decreases, with additional correlation. This change is likely related to the difficulty in accurately calculating $\tilde{B}$-state methyl torsional barriers, as discussed below. As expected, the $\tilde{B}$-state geometries of plain vinoxy and of the C_1C_2O frame of 1-methylvinoxy are very similar when computed at similar levels of theory. On the basis of the agreement between calculated and experimental rotational constants for plain vinoxy, we therefore suggest that the QRHF/EOMEE-CCSD $\tilde{B}$-state geometry in Table 7 is the most accurate.

Evidently, the primary effect of excitation from $\tilde{X}$ to $\tilde{B}$ for both plain vinoxy and 1-methylvinoxy is a *lengthening* of the CO bond by about 0.15 Å and a *shortening* of the frame CC bond (C_1C_2) by about 0.03 Å. In 1-methylvinoxy, the bond angle $C_3C_2C_1$ expands by almost 4°, whereas angle OC_2C_1 expands by 2.2°. These geometry changes partially explain the dramatic change in methyl torsional potential, as described next.

B. Methyl Torsional Potential. In earlier experimental and computational work on substituted toluenes and their cations,[11,19,51] we observed a strong correlation between the methyl rotor torsional potential and *differences in bond order* between the two CC bonds of the ring located *vicinal* to the rotor CH bonds. Asymmetric (ortho- or meta-) substitution of the ring and electronic excitation or ionization can cause substantial distortion of the ring. Across many examples, the preferred rotor conformation always places one CH bond cis to the vicinal ring CC bond of higher order (greater double-bond character), analogous to the preference in 2-methylpropene.

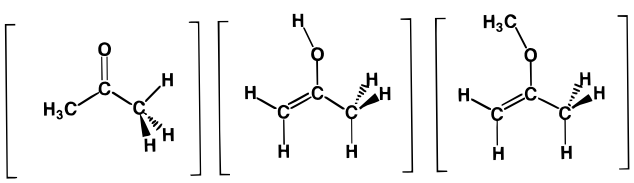

1. 2. 3.

A similar effect may contribute to the behavior of 1-methylvinoxy. The vicinal bonds of the frame are now C_1C_2 and C_2O. We have less experience with this situation, but a series of RHF/6-31++G** calculations on closed-shell molecules including acetone (**1**), 2-propenyl alcohol (**2**) (the enol corresponding to acetone), and methyl-2-propenyl ether (**3**) provide a semiquantitative guide. All three examples place a methyl rotor between a CC and CO bond with near-integral bond orders that differ from case to case. For **1** (calculated $V_3 = +224$ cm^{-1}), the preferred conformation is cis to the CO double bond. The ether **3** ($V_3 = -827$ cm^{-1}) places methyl between a single CO bond and a double CC bond. The preference for the rotor CH bond trans to CO (cis to the CC double bond) is even stronger than in 2-methylpropene ($V_3 = -690$ cm^{-1}).[52] As a final example, **2** shows an even stronger preference ($V_3 = -1023$ cm^{-1}).

Using these calculated barriers for stable molecules and the $\tilde{B} \leftarrow \tilde{X}$ geometry changes in 1-methylvinoxy, we can attempt to understand the methyl torsional potentials in 1-methylvinoxy as a competition between two effects. Double-bond character in C_2O pushes V_3 toward *positive* values (rotor CH cis to C_2O), whereas double-bond character in C_1C_2 pushes V_3 toward *negative* values (rotor CH trans to C_2O or cis to C_1C_2). In fact, for the five species **1**−**3** plus the $\tilde{X}$ and $\tilde{B}$ states of 1-methylvinoxy, there is a strong, monotonic correlation between V_3 and the difference in calculated *bond lengths*, $R_{cc} - R_{co}$. That difference serves here as a proxy for the difference in bond orders. The change in methyl rotor preferred orientation from cis to C_2O in the $\tilde{X}$ state to trans to C_2O in the $\tilde{B}$ state may be due, in part, to the substantial lengthening of C_2O and the modest shortening of C_1C_2 on electronic excitation.

However, we have also carried out CAS+1+2 calculations on the $\tilde{B}$ state for geometries in which the C_2O and C_1C_2 bond lengths are varied systematically and constrained to be substantially different from the equilibrium geometry. In fact, the change in barrier height for these geometries runs *counter* to the correlation described above, especially for the C_2O bond. The most likely explanation for this is that, in the excited state, the difference in bond lengths may not be a good proxy for the difference in bond orders. More detailed analysis of the interplay of these effects remains a worthy goal of future research.

VII. Conclusions

Once again, we find in both the $\tilde{X}$ and $\tilde{B}$ states of 1-methylvinoxy that the methyl rotor barrier is highly dependent on the local electronic structure of the frame to which it is attached. Calculated methyl rotor barriers for this radical are remarkably sensitive to basis set and level of theory, especially in the $\tilde{B}$ state. The excited-state barrier increases substantially from CASSCF to CAS+1+2 to coupled-cluster methods. The physical reason for the extreme difficulty in obtaining accurate calculated rotor barriers is not obvious. We note, in passing, that even the highest levels of theory explored here do not accurately reproduce the experimental CO stretching frequency in the $\tilde{B}$ state of 1-methylvinoxy; a similar difficulty occurs for plain vinoxy as well. Perhaps vibronic coupling to another electronic state is important. Meanwhile, all three treatments obtain reasonable electronic excitation energies (section V) and vibrational frequencies (Table 2). Our results thus serve as a cautionary note.

Acknowledgment. J.C.W. and L.B.H. thank the Department of Energy, Office of Basic Energy Sciences, Division of Chemical Sciences for generous support of this work (Grant DE-FG02-92ER14306 and Contract No. W-31-109-Eng-38, respectively). J.F.S. thanks the National Science Foundation

(CHE98-73818) for support. J.C.W. and S.W. acknowledge many helpful discussions with Prof. Frank Weinhold. J.C.W. also thanks Prof. C. Bradley Moore, his Ph.D. advisor, for his encouragement and his fine example over the years.

References and Notes

(1) Quandt, R.; Min, Z.; Wang, X.; Bersohn, R. *J. Phys. Chem. A* **1998**, *102*, 60.
(2) Schmoltner, A. M.; Chu, P. M.; Brudzynski, R. J.; Lee, Y. T. *J. Chem. Phys.* **1989**, *91*, 6926.
(3) Williams, S.; Zingher, E.; Weisshaar, J. C. *J. Phys. Chem. A* **1998**, *102*, 2297−2301.
(4) Washida, N.; Inomata, S.; Furubayashi, M. *J. Phys. Chem. A* **1998**, *102*, 7924−7930.
(5) Reed, A. E.; Weinhold, F. *Isr. J. Chem.* **1991**, *31*, 277.
(6) Johnson, P. M.; Sears, T. J. *J. Chem. Phys.* **1999**, *111*, 9222.
(7) Yu, L.; Cullin, D. W.; Williamson, J. M.; Miller, T. A. *J. Chem. Phys.* **1991**, *95*, 804.
(8) Brock, L. R.; Rohlfing, E. A. *J. Chem. Phys.* **1997**, *106*, 10048.
(9) Inoue, G.; Akimoto, H. *J. Chem. Phys.* **1980**, *74*, 425.
(10) DiMauro, L. F.; Heaven, M.; Miller, T. A. *J. Chem. Phys.* **1984**, *81*, 2339−2346.
(11) Lu, K.-T.; Weinhold, F.; Weisshaar, J. C. *J. Chem. Phys.* **1995**, *102*, 6787.
(12) Furubayashi, M.; Bridier, I.; Inomata, S.; Washida, N.; Yamashita, K. *J. Chem. Phys.* **1997**, *106*, 6302−6309.
(13) Bunker, P. R. *Molecular Symmetry and Spectroscopy*; Academic: New York, 1979.
(14) Longuet-Higgins, H. C. *Mol. Phys.* **1963**, *6*, 445.
(15) Walker, R. A.; Richard, E. C.; Lu, K.-T.; Weisshaar, J. C. *J. Phys. Chem.* **1995**, *99*, 12422.
(16) Lu, K.-T.; Weisshaar, J. C. *J. Chem. Phys.* **1993**, *99*, 4247.
(17) Lu, K.-T.; Eiden, G. C.; Weisshaar, J. C. *J. Phys. Chem.* **1992**, *96*, 9742.
(18) Lin, C. C.; Swalen, J. D. *Rev. Mod. Phys.* **1959**, *31*, 841.
(19) Richard, E. C.; Walker, R. A.; Weisshaar, J. C. *J. Chem. Phys.* **1995**, *104*, 4451.
(20) Barnhard, K. I.; He, M.; Weiner, B. R. *J. Phys. Chem.* **1996**, *100*, 2784−2790.
(21) Yamaguchi, M. *Chem. Phys. Lett.* **1994**, *221*, 531−536.
(22) Zhao, Z.-Q.; Parmenter, C. S.; Moss, D. B.; Bradley, A. J.; Knight, A. E. W.; Owens, K. G. *J. Chem. Phys.* **1992**, *96*, 6362.
(23) Ikoma, H.; Takazawa, K.; Emura, Y.; Ikeda, S.; Abe, H.; Hayashi, H.; Fujii, M. *J. Chem. Phys.* **1996**, *105*, 10201.
(24) Parmenter, C. S.; Stone, B. M. *J. Chem. Phys.* **1986**, *84*, 4710.
(25) Osborn, D. L.; Choi, H.; Mordaunt, D. H.; Bise, R. T.; Neumark, D. M.; Rohlfing, C. M. *J. Chem. Phys.* **1997**, *106*, 3049.
(26) Dupuis, M.; Wendoloski, J. J.; Lester, J. W. A. *J. Chem. Phys.* **1981**, *76*, 488.
(27) Dunning, T. H., Jr. *J. Chem. Phys.* **1989**, *90*, 1007.
(28) Kendall, R. A.; Dunning, T. H., Jr. *J. Chem. Phys.* **1992**, *96*, 6796.
(29) Woon, D. E.; Dunning, T. H., Jr. *J. Chem. Phys.* **1993**, *98*, 1358.
(30) Frisch, M. J.; Trucks, G. W.; Schlegel, H. B.; Scuseria, G. E.; Robb, M. A.; Cheeseman, J. R.; Zakrzewski, V. G.; Montgomery, J. A., Jr.; Stratmann, R. E.; Burant, J. C.; Dapprich, S.; Millam, J. M.; Daniels, A. D.; Kudin, K. N.; Strain, M. C.; Farkas, O.; Tomasi, J.; Barone, V.; Cossi, M.; Cammi, R.; Mennucci, B.; Pomelli, C.; Adamo, C.; Clifford, S.; Ochterski, J.; Petersson, G. A.; Ayala, P. Y.; Cui, Q.; Morokuma, K.; Malick, D. K.; Rabuck, A. D.; Raghavachari, K.; Foresman, J. B.; Cioslowski, J.; Ortiz, J. V.; Stefanov, B. B.; Liu, G.; Liashenko, A.; Piskorz, P.; Komaromi, I.; Gomperts, R.; Martin, R. L.; Fox, D. J.; Keith, T.; Al-Laham, M. A.; Peng, C. Y.; Nanayakkara, A.; Gonzalez, C.; Challacombe, M.; Gill, P. M. W.; Johnson, B. G.; Chen, W.; Wong, M. W.; Andres, J. L.; Head-Gordon, M.; Replogle, E. S.; Pople, J. A. *Gaussian 98*, revision A.6; Gaussian, Inc.: Pittsburgh, PA, 1998.
(31) Shepard, R.; Shavitt, I.; Pitzer, R. M.; Comeau, D. C.; Pepper, M.; Lischka, H.; Szalay, P. G.; Ahlrichs, R.; Brown, F. B.; Zhao, J.-G. *Int. J. Quantum Chem.* **1988**, *S22*, 149.
(32) Molpro is a package of ab initio programs written by H.-J. Werner and P. J. Knowles with contributions from J. Almlof, R. D. Amos, A. Berning, D. L. Cooper, M. J. O. Deegan, A. J. Dobbyn, F. Eckert, S. T. Elbert, C. Hampel, R. Lindh, A. W. Lloyd, W. Meyer, A. Nicklass, K. Peterson, R. Pitzer, A. J. Stone, P. R. Taylor, M. E. Mura, P. Pulay, M. Schutz, H. Stoll, and Thorsteinsson.
(33) Knowles, P. J.; Werner, H.-J. *Chem. Phys. Lett.* **1985**, *115*, 259.
(34) Werner, H.-J.; Knowles, P. J. *J. Chem. Phys.* **1985**, *82*, 5053.
(35) Stanton, J. F.; Gauss, J.; Watts, J. D.; Lauderdale, W. J.; Bartlett, R. J. *Int. J. Quantum Chem.* **1992**, *26*, 879.
(36) Werner, H.-J.; Knowles, P. J. *J. Chem. Phys.* **1988**, *89*, 5803.
(37) Knowles, P. J.; Werner, H.-J. *Chem. Phys. Lett.* **1988**, *145*, 514.
(38) Langkoff, S. R.; Davidson, E. R. *Int. J. Quantum Chem.* **1974**, *8*, 61.
(39) Silver, D. W.; Davidson, E. R. *Chem. Phys. Lett.* **1978**, *52*, 403.
(40) Purvis, G. D.; Bartlett, R. J. *J. Chem. Phys.* **1982**, *76*, 7918.
(41) Raghavachari, K.; Trucks, G. W.; Head-Gordon, M.; Pople, J. A. *Chem. Phys. Lett.* **1989**, *157*, 479.
(42) Noga, J.; Bartlett, R. J. *J. Chem. Phys.* **1990**, *165*, 512.
(43) Watts, J. D.; Bartlett, R. J. *J. Chem. Phys.* **1990**, *93*, 6104.
(44) Chiles, R. A.; Dykstra, C. E. *J. Chem. Phys.* **1981**, *74*, 4544.
(45) Rittby, M.; Bartlett, R. J. *J. Phys. Chem.* **1988**, *92*, 3033.
(46) Stanton, J. F.; Bartlett, R. J. *J. Chem. Phys.* **1993**, *98*, 7029.
(47) Although it is known that ground-state CC methods are relatively insensitive to the choice of orbitals and can provide good results even in cases of relatively severe spin contamination or unphysical localization of spin, the same is not true for excited-state studies. It has recently been demonstrated [Szalay, P. G.; Gauss, J. *J. Chem. Phys.* **2000**, *112*, 4027.] that relatively poor excited-state descripitons can be obtained for open-shell systems with EOMEE-CC methods when the ground-state reference determinant suffers from spin-contamination problems. The ultimate reason for this is that final-state orbital relaxation is not treated as well at the EOMEE-CC level as it is in the underlying CC calculation, so one must be more cautious about the choice of orbitals for excited-state calculations. At the B-state geometries, ground-state unrestricted Hartree−Fock wave functions have values of $\langle S^2 \rangle$ in the range of 1.0−1.1, indicative of strong spin contamination. Restricted open-shell Hartree−Fock orbitals for 1-methylvinoxy also turn out to be a poor choice; large single-excitation amplitudes were observed in the corresponding CCSD wave function. By this criteria (magnitude of largest single-excitation amplitudes), QRHF orbitals are superior to either unrestricted or restricted open-shell Hartree−Fock orbitals for the present purpose.
(48) Stanton, J. F. *J. Chem. Phys.* **1994**, *101*, 374.
(49) Although the four lowest molecular orbitals were frozen in the CCSDT calculations, this apparently has only a small effect on the barrier height. Freezing the core orbitals reduces the QRHF-CCSD(T) barrier by only 2 cm^{-1}, from 606 to 604 cm^{-1}.
(50) The optimizations were carried out with analytic gradients, and the harmonic frequencies were calculated by finite difference of analytic gradients. Although this is the first time that analytic QRHF/EOMEE-CCSD derivatives have been used, the underlying theory (Stanton, J. F. *J. Chem. Phys.* **1993**, *99*, 8840 for EOMEE-CCSD gradients and Gauss, J.; Stanton, J. F.; Bartlett, R. J. *J. Chem. Phys.* **1991**, *95*, 2629 for QRHF orbital relaxation effects) is well-known, and the implementation was relatively straightforward.
(51) Feldgus, S. H.; Schroeder, M. J.; Walker, R. A.; Woo, W.-K.; Weisshaar, J. C. *Int. J. Mass Spectrom. Ion Processes* **1996**, *159*, 231.
(52) Durig, J. R.; Guirgis, G. A.; Bell, S. *J. Phys. Chem.* **1989**, *93*, 3487.